

Supplementary Information

Surface Roughness Boosts SERS Performance of Imprinted Plasmonic Architectures

*Gerard Macias, María Alba, Lluís F. Marsal and Agustín Mihi**

Contents

- Fabrication**.....3
- Structural characterization**5
- Optical characterization**6
- Enhancement factor (EF) calculation**.....8
- Roughness effect**.....10
- Sample variability**.....11
- Simulations**.....11
- Assignment of vibrational normal modes**.....12
- References**.....15
- Annex I. Detailed enhancement factors of the devices studied**16

Fabrication

Glass substrate preparation

Glass substrates (25x25 mm) were cleaned in an ultrasonic bath first with a mixture of soap and DI water for 10 min, then with acetone for 10 min, ethanol for another 10 min and finally DI water for 10 min also. The clean substrates were then dried under a stream of air prior to hydroxylation in Piranha solution at 80 °C for 45 min. Then, hydroxylated substrates were rinsed with copious DI water and dried under a stream of air.

Rough photonic crystal fabrication (r-PC)

To prepare rough photonic crystals, an anatase titania 20nm-nanoparticle paste (90T, Dyesol) was spin-coated onto the cleaned glass substrates at 2000 rpm for 10 s. The titania-coated glass was then pressed against the PDMS master stamp and a weight was placed on top of the stamp to maintain the pressure while heated at 40 °C for 10 min. Subsequently, the PDMS stamp was carefully peeled off and the resulting imprinted titania films were baked at 450 °C for 2 h. This annealing step removes the organic part of the paste, leaving only sintered titania nanoparticles, producing some shrinkage in the nanodomains but maintaining the center to center distance. Finally, a thin Ag coating of 50 nm was sputtered on top of the structure and the resulting SERS substrates stored in N₂ for a later use.

Smooth photonic crystal fabrication (s-PC)

Smooth photonic crystals were prepared nanoimprinting an SU-8 (2000.5 Microchem) photoresist film spin casted and soft baked on a glass substrate, as described elsewhere¹. Ag coating of 50 nm was sputtered on top of the UV cured nanoimprinted film and the resulting SERS substrates stored in N₂ until used.

Table S1 shows a summary of the SERS devices studied in the present work, describing the device composition, nanostructure and resonance position of the crystal measured on the reflectance spectra.

Table S1. Summary of the structural and optical characteristics of SERS devices

Label	Description	Cylinder Diameter (nm)	Pitch (nm)	Resonance Position (nm)
s-F	Ag coated resist film on glass	N.A.	N.A.	N.A.
r-F	Ag coated TiO ₂ film on glass	N.A.	N.A.	N.A.
s-PC1	Ag coated resist PC on glass	300	580	600
r-PC1	Ag coated TiO ₂ PC on glass	300	580	600
s-PC2	Ag coated resist PC on glass	440	740	780
r-PC2	Ag coated TiO ₂ PC on glass	440	740	780

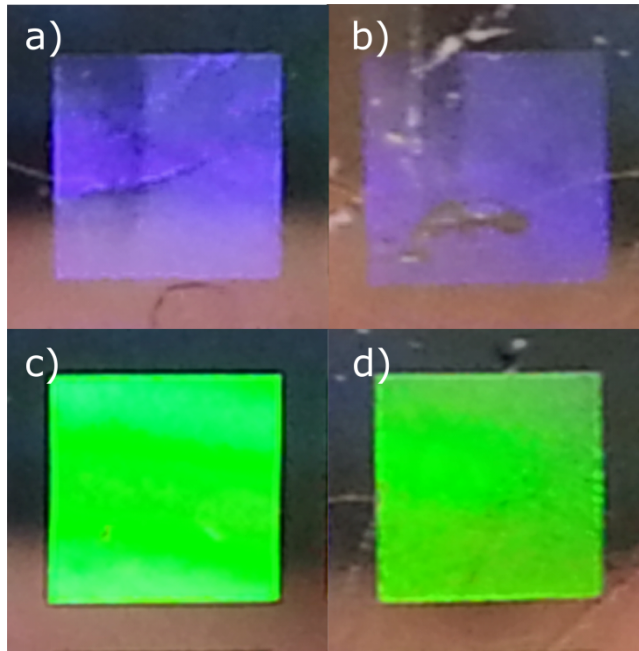


Figure S1. Photographs of the Plasmonic Crystals used in this study. s-PC1 (a), r-PC1 (b), s-PC2 (c) and r-PC2 (d). Plasmonic crystal size is 4x4mm.

Structural characterization

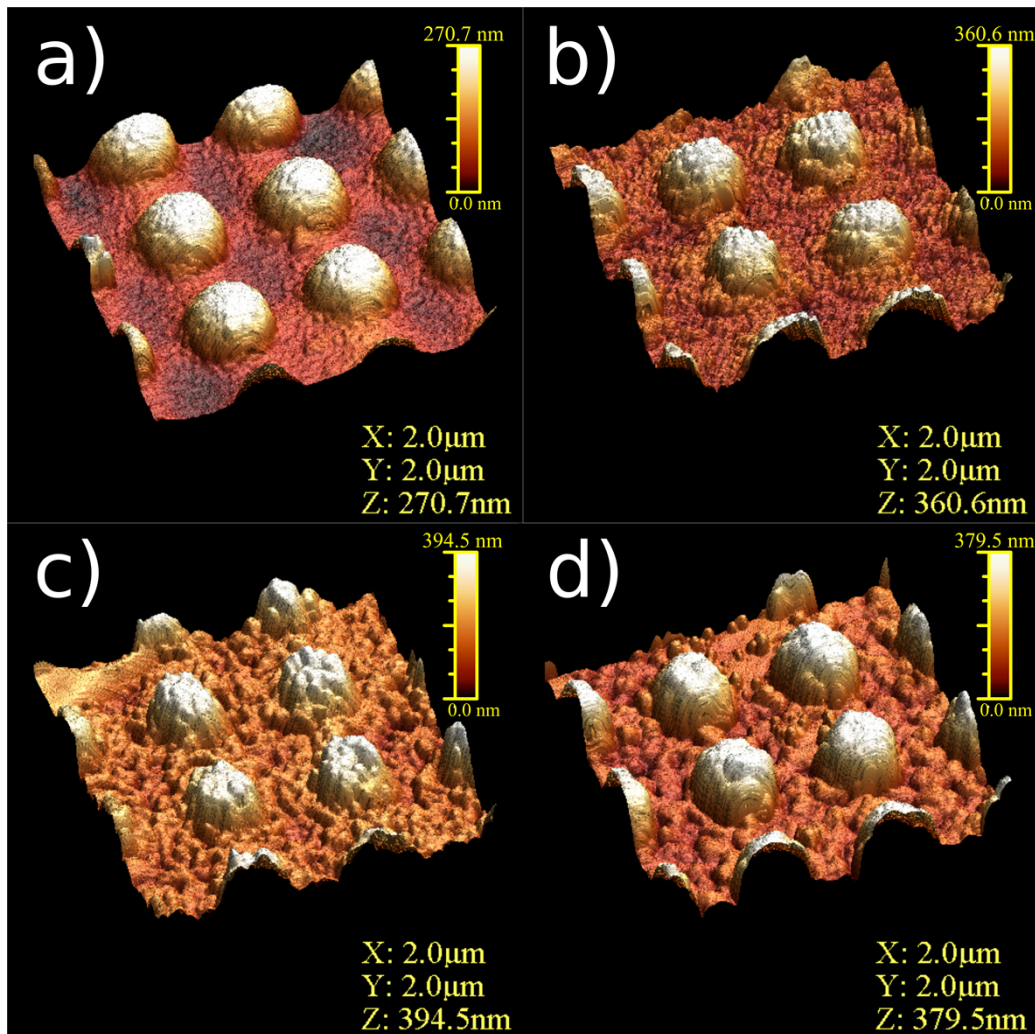


Figure S2. AFM characterization of 2D nanodome arrays. a) s-PC2, b) TiO_2 -PC, c) r-PC2 with 50 nm Ag, and d) r-PC2 with 100 nm Ag.

Figure S2 shows the 3-D rendering (www.wsxmsolutions.com) of the AFM data measured from 4 different plasmonic crystals: s-PC2, TiO_2 -2D (i.e. r-PC2 without Ag coating), r-PC2 coated with 50 nm of Ag and r-PC2 coated with 100 nm of Ag. It can be seen how the nanoscale roughness is higher in photonic crystals fabricated with the titania nanoparticle paste and how this surface roughness is diminished by increasing the Ag coating. Table S2 shows the results from the AFM analysis. The roughness mean squares (RMS) and roughness average (Ra) were measured at the interstices of the nanodome array.

Table S2. AFM roughness analysis and surface area. The Fill factors were calculated considering a unit cell of a square array of nanodomains with the diameter and pitch L summarized in table S1.

Sample	Fill factor	RMS (nm)	Ra (nm)	Surface Area (μm^2)
s-F	1.13	12.50	10.20	4.51
s-PC1	1.55	5.79	4.70	6.18
s-PC2	2.18	4.41	3.55	8.72
TiO ₂ -PC2	3.19	15.51	12.67	12.76
r-F	1.73	22.99	18.64	6.93
r-PC1	2.16	16.83	13.20	8.64
r-PC2 _{50nm Ag}	3.16	20.98	17.48	12.64
r-PC2 _{100nm Ag}	3.01	17.11	13.71	12.04

Optical characterization

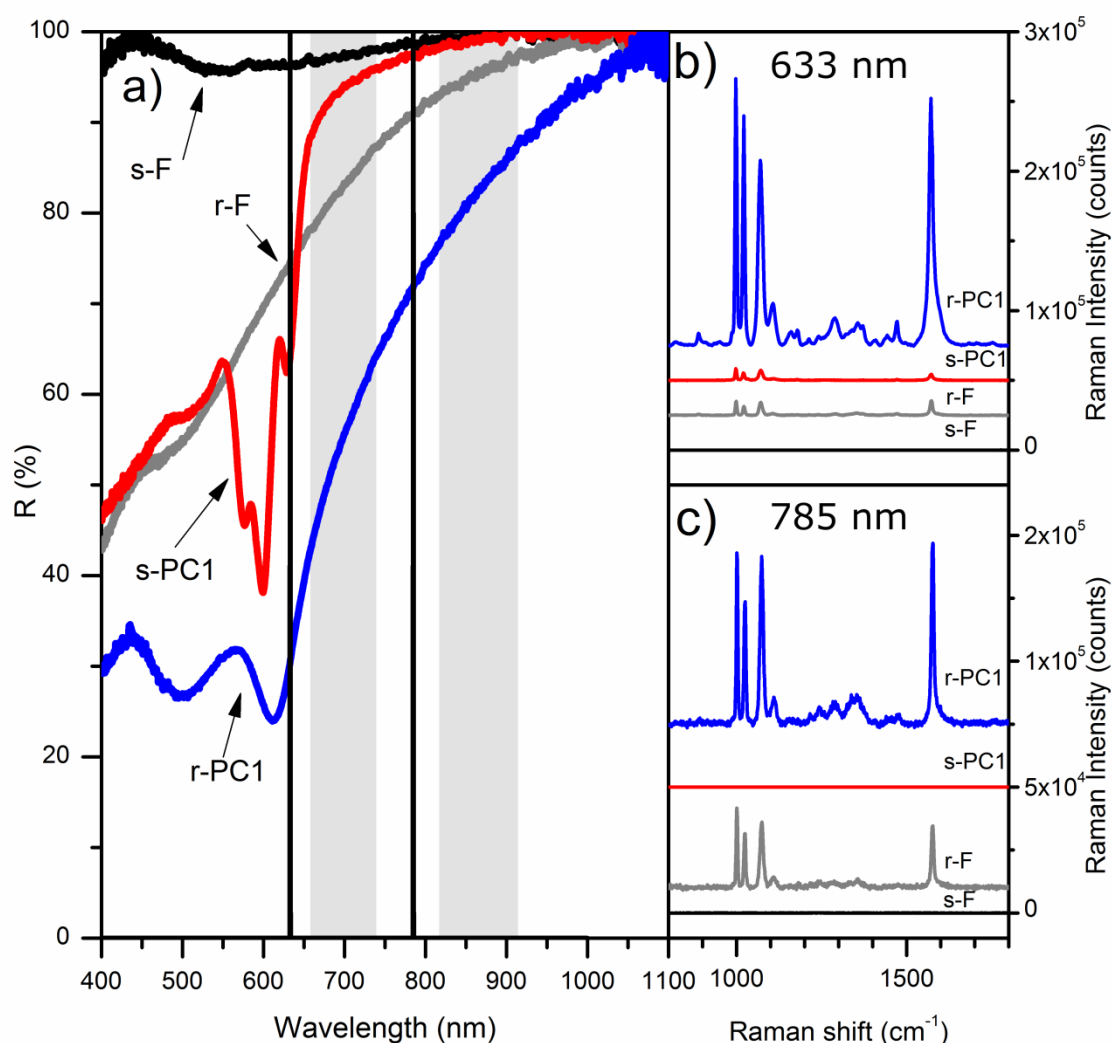


Figure S3. Optical characterization of Plasmonic Crystals. a) Reflectance spectra corresponding to a flat Ag film onto resist (s-F, black line), Ag film coated onto a TiO₂ film (r-F, grey line), Ag films onto a nanoimprinted resist (s-PC1, red line) and a Ag films onto a

nanoimprinted TiO₂ films (r-PC1, blue line). The excitation wavelengths ($\lambda_0 = 633$ and 785 nm) are depicted by vertical solid lines and the resulting Raman emission region for each excitation is represented by the shaded areas. b) and c) show the resulting Raman spectra of each of the devices for the excitation wavelengths $\lambda_0 = 633$ nm and $\lambda_0 = 785$ nm, acquired through a 10x objective and 10s integrating time. The fingerprint spectral region of BZT is converted into wavelength from Raman shift following the expression in eq 1, for comparison with the reflectance spectra of the photonic architectures. In Equation S1, λ_1 is the wavelength at which Raman scattered photons are emitted, $\Delta\omega$ is the Raman shift and λ_0 is the excitation wavelength.

$$\lambda_1(nm) = \frac{-\lambda_0(nm)}{\frac{\Delta\omega(cm^{-1})\lambda_0(nm)}{10^7} - 1} \quad (1)$$

Figure S3 shows the optical characterization of Plasmonic Crystals s-PC1 and r-PC1. When the resist is shaped in a 2D nanodome array and coated with metal (s-PC1), the reflectance (Figure S3a, red line) presents well defined dips that correspond to the different resonant modes that this architecture can sustain; Bragg resonances coupled through the 2D grating and the localized resonances of the nanodomains. s-PC1 (Figure S3a, red line), presents SPPs centered at 600 nm. When the same architectures are fabricated using titanium dioxide, the resulting rough plasmonic crystal, r-PC1 (Figure S3a, blue line) presents lower reflectance and broadened spectral features as a result of the excitation of localized plasmon resonances arising from the surface roughness. In addition to the plasmonic resonances, the nanodome array also shows a high degree of light scattering below their Bragg-SPP resonance. This can be noticed by the difference between the specular reflectance and the reflectance obtained with an integrating sphere (figure S4).

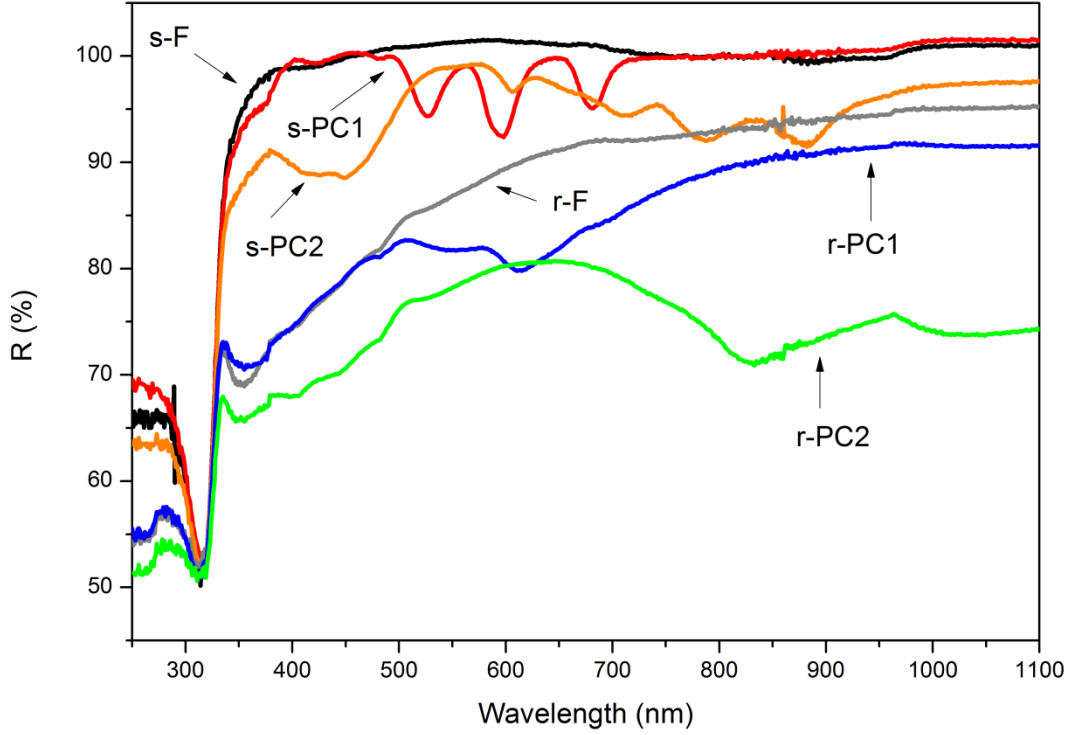


Figure S4. Reflectance spectra of plasmonic crystals measured with an integrating sphere. Reflectance of flat Ag film on photoresist (s-F, black line), Ag film coated onto a TiO₂ film (r-F, grey line), Ag films onto a nanoimprinted resist (s-PC1, red line and s-PC2, orange line) and a Ag films onto a nanoimprinted TiO₂ films (r-PC1, blue line and r-PC2, green line).

Enhancement factor (EF) calculation.

In order to quantify the performance of the SERS devices studied, the devices were functionalized with benzenethiol (BZT) by immersion in 3 mM benzenethiol solution in methanol overnight. Then the devices were cleaned with ethanol to remove non-adhered benzenethiol molecules, dried under a stream of air and subsequently measured in a Raman microscope (Renishaw Ltd.) using a 10x objective. Since the signal arising from SERS is related with the number of molecules adsorbed on the surface of the metal film, our EF calculation was based on the number of molecules excited according to the following expression:

$$EF = \left(\frac{I_{SERS}}{N_{SERS}} \right) \left(\frac{N_{neat}}{I_{neat}} \right) \quad (2)$$

Where I_{SERS} is the height of the Raman peak (maximum number of counts subtracting background) of the measured PC, I_{neat} is the height of the same Raman peak of liquid pure BZT, N_{SERS} is the number of BZT molecules in the PC contributing to the Raman signal (considering both the fill factor and the surface area of the PC) and N_{neat} is the number of molecules contributing to the Raman signal of pure BZT.

It can be observed how in all cases rough plasmonic crystals result in higher EFs with respect to smooth plasmonic crystals. Also, it can be noted how plasmonic crystals show an

increment in the EF with respect to planar films. Further details on the EFs calculated in this work are shown at the end of this Supporting Information document (Annex I, tables 1 and 2).

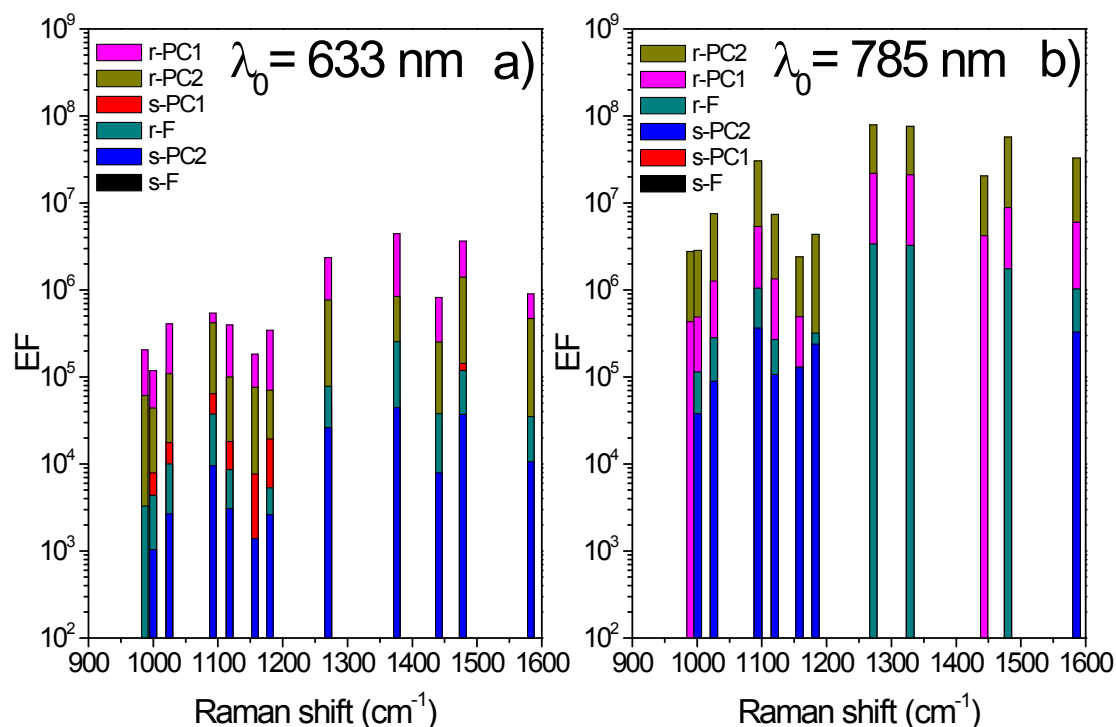


Figure S5. Experimental EF calculated from the Raman spectra measured from different SERS substrates for each Raman peak associated to different vibrational modes of the BZT molecule. r-F, s-F, r-PC1 and s-PC1 under a) excitation at $\lambda_0 = 633$ nm and b) excitation at $\lambda_0 = 785$ nm.

Figure S5 shows the resulting EF of all the studied SERS substrates. Note that s-F devices show no EF as no peak could be observed in the Raman spectrum. It can be observed how, in general, excitation at 785 nm results in higher EFs with respect to excitation at 633 nm. It can be noted that rough plasmonic crystals show Raman signal at both excitation wavelengths while smooth plasmonic crystals show signal only at wavelengths below their plasmonic resonance due to the higher hot spot density in rough photonic crystals arising from the nanoscale roughness. However, it can be observed how the best performance at each excitation wavelengths studied corresponds to the photonic crystal (rough or smooth) with the plasmonic resonance designed for that specific wavelength.

Roughness effect

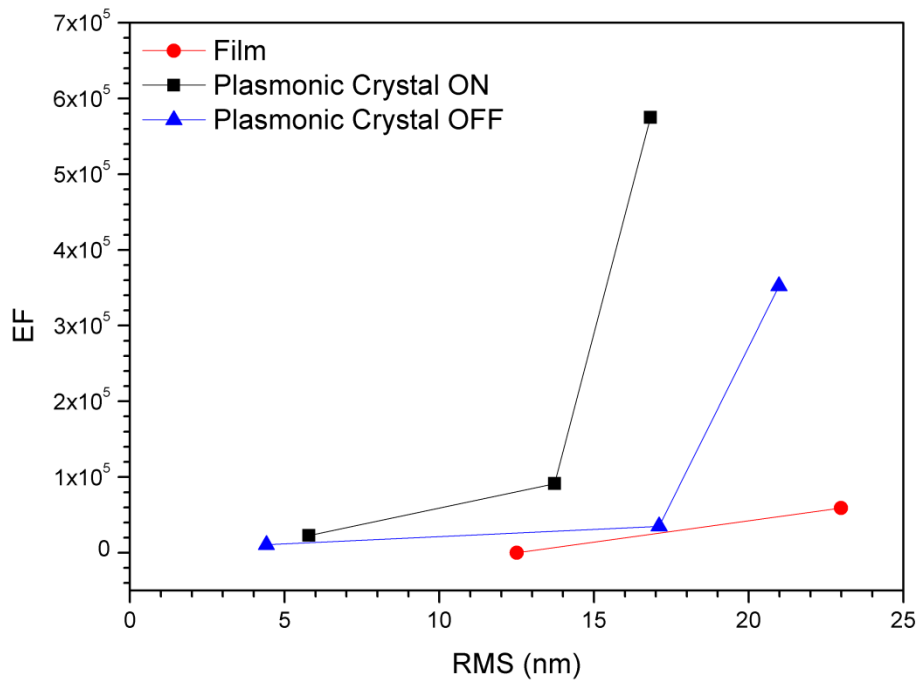


Figure S6. Correlation of surface roughness with the EF. Red circles show the correlation of the EF with nanoscale roughness on planar Ag films, black squares show the relationship of EF with RMS in plasmonic crystals excited at the SPP resonance, and blue triangles shows the effect of roughness on the EF in plasmonic crystals excited outside the SPP resonance.

In figure S5 it has been observed that rough photonic crystals display a better EF than smooth photonic crystals. Figure S6 illustrates the correlation of the surface roughness with the average EF on both planar films and photonic crystals in resonance (i.e. ON state) and out of resonance (i.e. OFF state). It can be observed how increasing surface roughness increases the achieved EF in all cases. However, it can also be observed that this increment is much more noticeable for imprinted plasmonic crystals than planar films and that excitation at the SPP resonance enhances the effect of the nanoscale roughness even further.

Sample variability

One important factor for the development of successful SERS devices is the repeatability of the Raman intensity measured. Figure S7 shows the distribution of the Raman intensity band at 1000 cm^{-1} superimposed on an optical microscopy image of the region analyzed. It can be observed how the Raman Intensity in the rough photonic crystal is homogeneously distributed along the imprinted region. Moreover, it can be noted the difference in the intensity of the Raman signal between the rough flat area (i.e. the dark region in the Raman scattering map) and the imprinted r-PC region (in red).

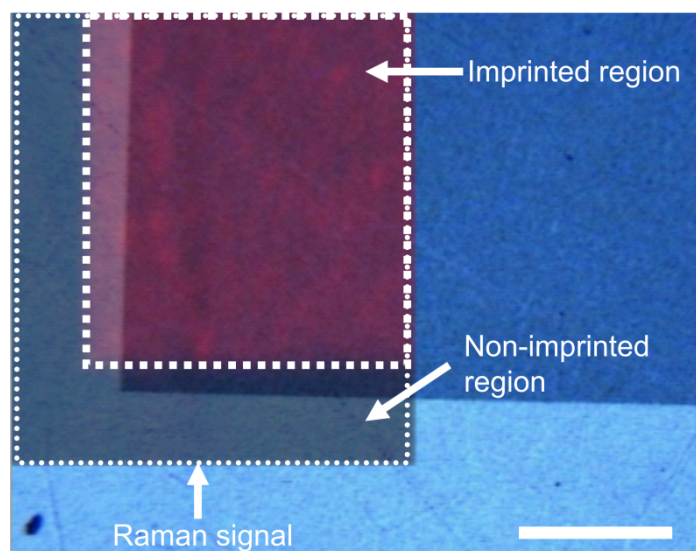


Figure S7. Intra-device repeatability at 1000 cm^{-1} . Superimposed Raman scattering distribution of the vibrational band at 1000 cm^{-1} obtained at $\lambda_0 = 785\text{ nm}$ excitation wavelength with optical microscopy photograph of a r-PC2 SERS device. The dotted region shows the Raman signal obtained from the corner of the plasmonic crystal (Raman scattering map and optical micrograph displacement is due to distinct optical paths during the acquisition). Scale bar is $100\mu\text{m}$.

Simulations

Electric Field Intensity Modeling. Finite-difference time-domain simulations (FDTD) were carried out using Lumerical FDTD solutions suite version 8 (<http://www.lumerical.com>). Briefly, A unit cell (2nm resolution) illuminated with a plane-wave source was simulated with symmetric and antisymmetric boundary conditions. The rough and smooth PC geometries were imported from the AFM data (1nm resolution, 2microns x 2 microns) and considered a 50nm silver coating (refractive index from Johnson and Christy).

Assignment of vibrational normal modes

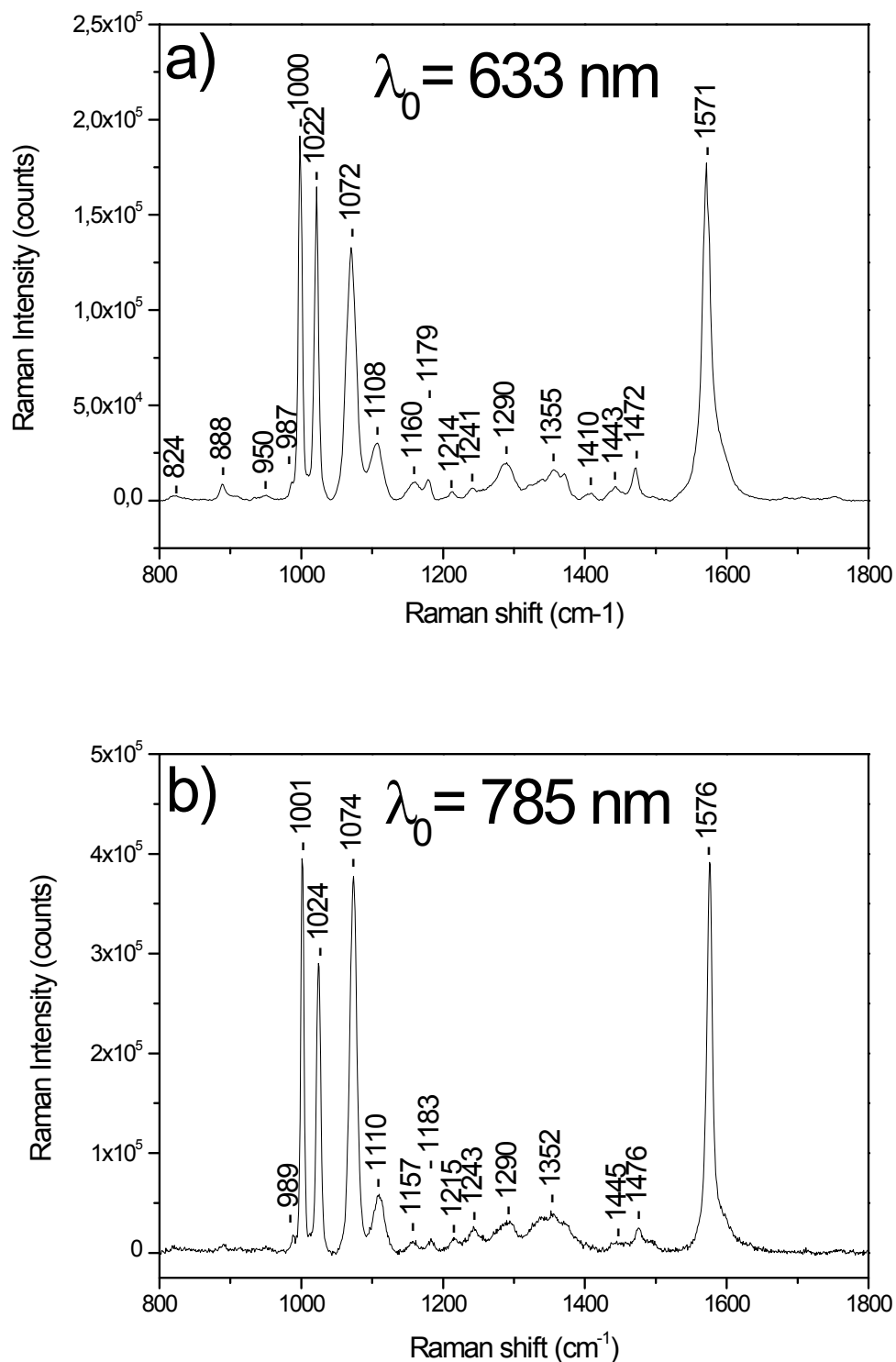


Figure S8. Raman spectrum of BZT adsorbed to a r-PC under two different excitations: a) $\lambda_0 = 633 \text{ nm}$, and b) $\lambda_0 = 785 \text{ nm}$.

Table S3. Vibrational normal modes of BZT assigned for excitation wavelengths of $\lambda_0 = 633$ nm and $\lambda_0 = 785$ nm and their associated EFs.

Neat Raman shift at 633 nm (cm^{-1})	r-PC1 Raman shift* at 633 nm (cm^{-1})	EF	Neat Raman shift at 785 nm (cm^{-1})	r-PC2 Raman shift* at 785 nm (cm^{-1})	EF	Assignment**
	824	N/A			N/A	v10b
	880	N/A			N/A	v17b
916		N/A			N/A	$\delta(\text{SH})$
	950	N/A			N/A	v17a
987	987(0)	2,10E+05	990	989(-1)	2,80E+06	v5
1000	1000(0)	1,20E+05	1001	1001(0)	2,80E+06	v12
1025	1022(-3)	4,10E+05	1026	1024(-2)	7,50E+06	v18a
1092	1072(-20)	5,40E+05	1094	1074(-20)	3,00E+07	v1
1118	1108(-10)	4,00E+05	1120	1110(-10)	7,40E+06	v6a+ v7a
1157	1160(+3)	1,80E+05	1158	1157(-1)	2,40E+06	v9b
1180	1179(-1)	3,40E+05	1183	1183(0)	4,30E+06	v9a
	1214	N/A		1215	N/A	v6a overtone
	1241	N/A		1243	N/A	v7a overtone
1270	1290(+20)	2,40E+06	1272	1290(+18)	7,90E+07	v3
1376	1355(-21)	4,40E+06	1329	1352(+23)	7,60E+07	v14
	1410	N/A			N/A	v12+v(CS) + v(AgS)
1441	1443(-2)	8,20E+05	1443	1445(+2)	2,10E+07	v19a
1478	1472(-6)	3,70E+06	1476	1476(-4)	5,70E+07	v19b
1583	1571(-12)	9,00E+05	1586	1576(-10)	3,30E+07	v8a

*Numbers in parenthesis show the position shift between the neat BZT and BZT adsorbed onto the plasmonic crystal.

** Assignments based on Wilson's notation.^[2]

The vibrational analysis of BZT shows a total of 18 vibrational bands in r-PC1 and 14 vibrational bands for r-PC2 within the same spectral region. The assignments of the Raman bands of BZT_{neat}, r-PC1 and r-PC2 are presented in table S3. This higher amount of peaks upon illumination at 633 nm may be attributed to a better excitation of the vibrational normal modes due to excitation at a wavelength where BZT displays a higher absorption. The band not shown in r-PC and located at 917 cm^{-1} in the BZT neat spectrum and corresponds to the in-plane deformation of the thiol group ($\delta(\text{SH})$). This disappearance is expected for r-PC, as BZT reacts with Ag to form a silver phenylthiolate complex.^[3] The extra vibrational modes not visible in the BZT neat spectrum are attributed to vibrational normal modes that are normally too weak to be observed.^[4-5] This leaves a total of 12 vibrational bands to determine the EF of our rough PC. If we focus on the resulting EF of each of the 12 vibrational bands displayed in all the Raman spectra, we can notice that 6 bands are enhanced by $\sim 10^6$ and 6 bands are enhanced by $\sim 10^7$ in r-PC2 and a similar trend can be observed for r-PC1. Observing the position shift between the Raman peaks of BZT_{neat} and r-PC2, we can see that 4 out of the 6 vibrational normal modes enhanced by $\sim 10^7$ show a significant position shift (i.e. $\geq 10 \text{ cm}^{-1}$) in the spectrum of r-PC2 while just 1 of the 6 modes enhanced by $\sim 10^6$ show such a shift. This latter case corresponds to the combination of the bands v6a + v7a and the total 10

cm^{-1} difference may be attributed to the sum of individual smaller shifts of these two vibrational modes. A similar behaviour can be observed for r-PC1. From the results presented here, we can observe how the resulting EF is dependent on the vibrational normal mode analyzed. This may be attributed to the combination of the electromagnetic enhancement with a chemical enhancement where the molecular orientation of BZT with respect to the microstructured Ag surface plays a key role.

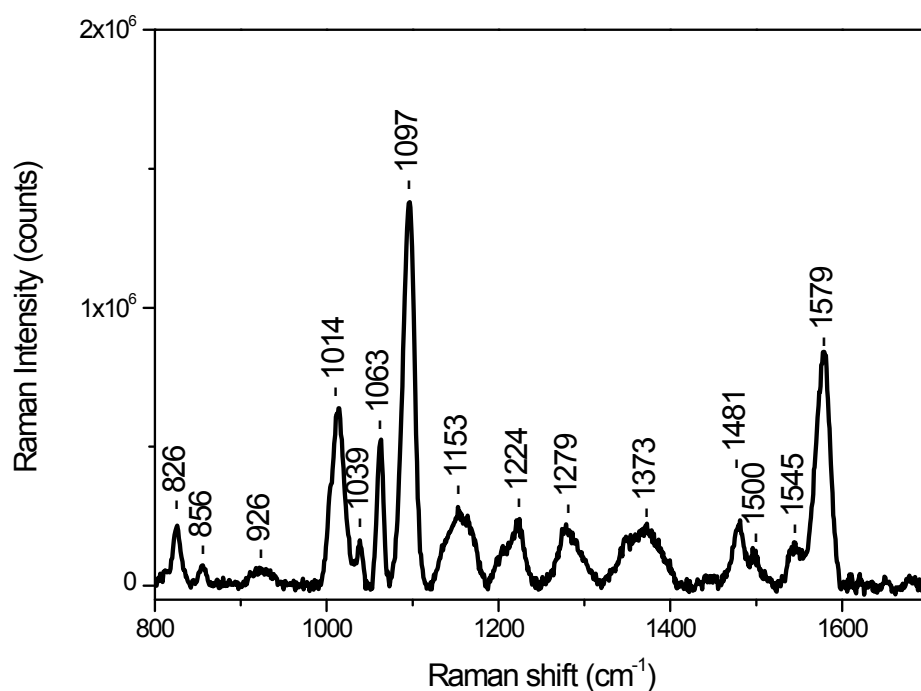


Figure S9. Raman spectrum of 4-MPy adsorbed onto a r-PC at $\lambda_0 = 785$ nm.

Table S4. Vibrational normal modes of 4-MPy assigned for an excitation wavelength of $\lambda_0 = 785$ nm and their associated EFs.

15 mM 4-MPy Raman shift at 785 nm (cm^{-1})	r-PC2 Raman shift at 785 nm (cm^{-1})	EF	Assignment*
	826		$\nu_{10b_1} + \delta(\text{C-H})$
	856		$\beta(\text{C-H})$
	926		$\nu_{5b_1} + \delta(\text{C-H})$
1002	1014(+12)	2,7E+09	ν_{1a_1}
	1039		ν_{18a_1}
1051	1063(+12)	1,0E+10	ν_{18b_2}
1116	1097(-19)	1,9E+10	ν_{12a_1}
	1153		$\nu_{5b_2} + \delta(\text{C-H})$
	1224		$\nu_{9b_{a_1}} + \beta(\text{C-H})$
	1279		$\nu_{3b_1} + \beta(\text{C-H})$
	1373		$\nu_{4b_2} + \nu(\text{CC})$
	1481		$\nu_{19b_2} + \nu(\text{C=C/C=N})$
	1500		$\nu_{9a_1} + \nu(\text{C=C/C=N})$

	1545		$\nu 8b_2 + \nu(CC)$
1623	1579(-44)	9,6E+09	$\nu 8a_1 + \nu(CC)$

*Assignments are based on references.^[6-8]

The vibrational analysis of 4-MPy revealed a total of 15 Raman peaks. Just 4 of these peaks (i.e. the most intense ones situated at 1002, 1051, 1116 and 1623 cm^{-1}) were visible in the reference spectrum of a 15 mM solution of 4-MPy in DI H₂O. Nevertheless, All the peaks appearing in the r-PC spectrum depicted in **Figure S9** could be attributed to vibrational normal modes of 4-MPy.^[5-8] The detailed assignments of the Raman peaks are shown in Table S4. Similar to the case of BZT, the highest EF achieved in 4-MPy vibrational modes appear when the bands display a higher shift between the position in the reference and the SERS spectra.

References

- [1] Mihi, F. J. Beck, T. Lasanta, A. K. Rath, G. Konstantatos, *Adv. Mater.* **2014**, *26*, 443.
- [2] E. B. Wilson, *Phys. Rev.* **1934**, *45*, 706.
- [3] S. Li, D. Wu, X. Xu, R. Gu, *J. Raman Spectrosc.* **2007**, *38*, 1436.
- [4] A. Szafranski, W. Tanner, P. E. Laibinis, R. L. Garrell, *Langmuir* **1998**, *14*, 3570.
- [5] G. T. Feugmo, V. Liégeois, *Chem. Phys. Chem.* **2013**, *14*, 1633.
- [6] J. Baldwin, N. Schühler, I. S. Butler, M. P. Andrews *Langmuir* **1996**, *12*, 1389.
- [7] Z. Wang, L. J. Rothberg, *J. Phys. Chem. B* **2005**, *109*, 3387.
- [8] L. Zhang, Y. Bai, Z. Shang, Y. Zhang, Y. Mo, *J. Raman. Spectrosc.* **2007**, *38*, 1106.

Annex I. Detailed enhancement factors of the devices studied

Table 1. Vibrational analysis of Raman spectra obtained from 2D nanodome arrays upon illumination at $\lambda_0 = 633$ nm, 3.4 mW and 10 s of integration time. EF calculated according to eq (1).

Neat			s-PC1				
Raman shift (cm ⁻¹)	Raman Intensity (counts)	Molecules	Raman shift (cm ⁻¹)	Raman Intensity (counts)	FF	Molecules	EF
919	2371,4	3,1E+12			1,55	7,9E+07	0,0E+00
987	2449,3						0,0E+00
1000	57967,6		998(-2)	8383,8			5,7E+03
1025	16128,0		1020(-5)	5205,1			1,3E+04
1092	6215,8		1072(-20)	7297,7			4,6E+04
1118	3832,5		1108(-10)	1270,4			1,3E+04
1157	2571,3		1159(+2)	361			5,5E+03
1180	1649,8		1179(-1)	586			1,4E+04
1270	339,9		1261(-9)	303,5			3,5E+04
1328	384,9						0,0E+00
1376	157,9		1362(-14)	166,3			4,2E+04
1441	366,8		1435(-6)	204,9			2,2E+04
1478	223,2		1471(-7)	582,2			1,0E+05
1583	7536,5		1573(-10)	4231,3			2,2E+04

Neat			s-PC2				
Raman shift (cm ⁻¹)	Raman Intensity (counts)	Molecules	Raman shift (cm ⁻¹)	Raman Intensity (counts)	FF	Molecules	EF
919	2371,4	3,1E+12			2,18	1,1E+08	0,0E+00
987	2449,3						0,0E+00
1000	57967,6		998(-2)	2153,4			1,0E+03
1025	16128,0		1022(-3)	1528,8			2,7E+03
1092	6215,8		1072(-20)	2106,3			9,5E+03
1118	3832,5		1108(-10)	419,5			3,1E+03
1157	2571,3		1156(-1)	127,4			1,4E+03
1180	1649,8		1179(-1)	154,2			2,6E+03
1270	339,9		1281(+11)	316,2			2,6E+04
1328	384,9						0,0E+00
1376	157,9		1370(+6)	250			4,4E+04
1441	366,8		1435(-6)	103,6			7,9E+03
1478	223,2		1472(-6)	296,3			3,7E+04
1583	7536,5		1573(-10)	2853,9			1,1E+04

Neat			r-F				
Raman shift (cm ⁻¹)	Raman Intensity (counts)	Molecules	Raman shift (cm ⁻¹)	Raman Intensity (counts)	FF	Molecules	EF
919	2371,4	3,1E+12			1,73	8,8E+07	0,0E+00
987	2449,3		985(-2)	316,3			4,6E+03
1000	57967,6		1000(0)	9921,6			6,1E+03
1025	16128,0		1022(-3)	6330,4			1,4E+04
1092	6215,8		1072(-20)	9156,7			5,2E+04
1118	3832,5		1108(-10)	1292,9			1,2E+04
1157	2571,3						0,0E+00
1180	1649,8		1182(+2)	345,2			7,4E+03
			1214	366,2			N/A
			1240	458,9			N/A
1270	339,9		1291(+21)	1044,4			1,1E+05
1328	384,9						0,0E+00
1376	157,9		1352(-24)	1589,5			3,6E+05
1441	366,8		1447(+6)	546,8			5,3E+04
1478	223,2		1472(-6)	1045,6			1,7E+05
1583	7536,5		1573(-10)	10378,4			4,9E+04

Neat			r-PC1				
Raman shift (cm ⁻¹)	Raman Intensity (counts)	Molecules	Raman shift (cm ⁻¹)	Raman Intensity (counts)	FF	Molecules	EF
919	2371,4	3,1E+12			2,16	1,1E+08	0,0E+00
987	2449,3		987(0)	9957,7			1,2E+05
1000	57967,6		1000(0)	135556,8			6,6E+04
1025	16128,0		1022(-3)	129944,2			2,3E+05
1092	6215,8		1172(-20)	66583,7			3,0E+05
1118	3832,5		1108(-10)	29935,7			2,2E+05
1157	2571,3		1160(+3)	9273,3			1,0E+05
1180	1649,8		1179(-1)	11181,6			1,9E+05
			1212	4632,3			N/A
			1241	5436,9			N/A
1270	339,9		1290(+20)	15907,8			1,3E+06
1328	384,9						0,0E+00
1376	157,9		1355(-21)	13813,9			2,5E+06
1441	366,8		1443(-2)	5939,5			4,6E+05
1478	223,2		1472(-6)	16156,1			2,1E+06
1583	7536,5		1571(-12)	134844,6			5,1E+05

Neat			r-PC2				
Raman shift (cm ⁻¹)	Raman Intensity (counts)	Molecules	Raman shift (cm ⁻¹)	Raman Intensity (counts)	FF	Molecules	EF
919	2371,4	3,1E+12			3,16	1,6E+08	0,0E+00
987	2449,3		987(0)	2956,6			6,1E+04
1000	57967,6		998(-2)	50230,3			4,4E+04
1025	16128,0		1022(-3)	34864,4			1,1E+05
1092	6215,8		1070(-22)	51427,8			4,2E+05
1118	3832,5		1108(-10)	7599,6			1,0E+05
1157	2571,3		1160(+3)	3883,7			7,6E+04
1180	1649,8		1180(0)	2298,2			7,0E+04
			1214	1237,9			N/A
1270	339,9		1284(+14)	5138,2			7,6E+05
1328	384,9						0,0E+00
1376	157,9		1353(-26)	2629			8,4E+05
1441	366,8		1435(-6)	1830,7			2,5E+05
1478	223,2		1472(-6)	6172,4			1,4E+06
1583	7536,5		1571(-12)	69950,2			4,7E+05

Table 2. Vibrational analysis of Raman spectra obtained from 2D nanodome arrays upon illumination at $\lambda_0 = 785$ nm, 5.6 mW and 10 s of integration time.

Neat			s-PC2				
Raman shift (cm ⁻¹)	Raman Intensity (counts)	Molecules	Raman shift (cm ⁻¹)	Raman Intensity (counts)	FF	Molecules	EF
917	1071	1,9E+13			2,18	1,7E+08	0,0E+00
990	1300,1						0,0E+00
1001	28011,9		1001(0)	9501,6			3,8E+04
1026	7736,7		1026(0)	6173,2			8,9E+04
1094	2507,2		1078(-16)	8182,3			3,6E+05
1120	1607,8		1117(-3)	1535,1			1,1E+05
1158	956,1		1159(+1)	1096,6			1,3E+05
1183	656,1		1179(-4)	1403,6			2,4E+05
1272	82,8						0,0E+00
1329	112,3						0,0E+00
1443	116,1						0,0E+00
1480	88,1						0,0E+00
1586	2408,2		1577(-9)	7107,1			3,3E+05

Neat			r-F				
Raman shift (cm ⁻¹)	Raman Intensity (counts)	Molecules	Raman shift (cm ⁻¹)	Raman Intensity (counts)	FF	Molecules	EF
917	1071	1,9E+13			1,73	1,4E+08	0,0E+00
990	1300,1						0,0E+00
1001	28011,9		1001(0)	31653,1			1,6E+05
1026	7736,7		1025(+1)	21515,2			3,9E+05
1094	2507,2		1075(-19)	26099,3			1,5E+06
1120	1607,8		1109(-11)	4273,7			3,7E+05
1158	956,1		1159(+1)	1234,5			1,8E+05
1183	656,1		1182(-1)	2064,7			4,4E+05
			1239	2697,8			N/A
1272	82,8		1287(+15)	2757,4			4,7E+06
1329	112,3		1358(+29)	3596,7			4,5E+06
1443	116,1						0,0E+00
1480	88,1		1474(-6)	1540			2,5E+06
1586	2408,2		1577(-9)	24546,3			1,4E+06

Neat			r-PC1				
Raman shift (cm ⁻¹)	Raman Intensity (counts)	Molecules	Raman shift (cm ⁻¹)	Raman Intensity (counts)	FF	Molecules	EF
917	1071	1,9E+13			2,16	1,7E+08	0,0E+00
990	1300,1		990(0)	2777,5			2,4E+05
1001	28011,9		1001(0)	67987,8			2,7E+05
1026	7736,7		1025(-1)	48593,6			7,1E+05
1094	2507,2		1074(-20)	66583,7			3,0E+06
1120	1607,8		1110(-10)	10672,7			7,5E+05
1158	956,1		1156(-2)	2333,8			2,8E+05
1183	656,1						0,0E+00
			1216	4157,7			N/A
			1244	6831,8			N/A
1272	82,8		1291(+19)	9001,3			1,2E+07
1329	112,3		1353(+24)	11725,7			1,2E+07
1443	116,1		1450(+7)	2409,8			2,3E+06
1480	88,1		1476(-4)	3868,8			5,0E+06
1586	2408,2		1577(-9)	71906,6			3,4E+06

Neat			r-PC2				
Raman shift (cm ⁻¹)	Raman Intensity (counts)	Molecules	Raman shift (cm ⁻¹)	Raman Intensity (counts)	FF	Molecules	EF
917	1071	1,9E+13			3,16	2,5E+08	0,0E+00
990	1300,1		989(-1)	17897,5			2,8E+06
1001	28011,9		1001(0)	395263,4			2,8E+06
1026	7736,7		1024(-2)	290065,8			7,5E+06
1094	2507,2		1073(-20)	377544,3			3,0E+07
1120	1607,8		1110(-10)	58943,8			7,4E+06
1158	956,1		1157(-1)	11436,4			2,4E+06
1183	656,1		1183(0)	14172,7			4,3E+06
			1215	15480,7			N/A
			1243	26534,6			N/A
1272	82,8		1290(+18)	32395,1			7,9E+07
1329	112,3		1352(+23)	42385,9			7,6E+07
1443	116,1		1445(+2)	11823,5			2,1E+07
1480	88,1		1476(-4)	24954,8			5,7E+07
1586	2408,2		1576(-10)	391705,7			3,3E+07